Zooplankton can actively adjust their motility to turbulent flow

François-Gaël Michalec[a,1], Itzhak Fouxon[a], Sami Souissi[b], and Markus Holzner[a]

[a]Institute of Environmental Engineering, Swiss Federal Institute of Technology, 8093 Zurich, Switzerland; and [b]Laboratoire d'Océanologie et de Géosciences, Université de Lille, CNRS, Université Littoral Côte d'Opale, UMR 8187, F 62930 Wimereux, France

Edited by M. A. R. Koehl, University of California, Berkeley, CA, and approved November 10, 2017 (received for review May 29, 2017)

Calanoid copepods are among the most abundant metazoans in the ocean and constitute a vital trophic link within marine food webs. They possess relatively narrow swimming capabilities, yet are capable of significant self-locomotion under strong hydrodynamic conditions. Here we provide evidence for an active adaptation that allows these small organisms to adjust their motility in response to background flow. We track simultaneously and in three dimensions the motion of flow tracers and planktonic copepods swimming freely at several intensities of quasi-homogeneous, isotropic turbulence. We show that copepods synchronize the frequency of their relocation jumps with the frequency of small-scale turbulence by performing frequent relocation jumps of low amplitude that seem unrelated to localized hydrodynamic signals. We develop a model of plankton motion in turbulence that shows excellent quantitative agreement with our measurements when turbulence is significant. We find that, compared with passive tracers, active motion enhances the diffusion of organisms at low turbulence intensity whereas it dampens diffusion at higher turbulence levels. The existence of frequent jumps in a motion that is otherwise dominated by turbulent transport allows for the possibility of active locomotion and hence to transition from being passively advected to being capable of controlling diffusion. This behavioral response provides zooplankton with the capability to retain the benefits of self-locomotion despite turbulence advection and may help these organisms to actively control their distribution in dynamic environments. Our study reveals an active adaptation that carries strong fitness advantages and provides a realistic model of plankton motion in turbulence.

zooplankton | turbulence | motility | particle-tracking velocimetry | biophysical coupling

The interplay between turbulence and the motility of plankton is an intriguing subject for investigation for both the ecology and physics communities, particularly since recent developments in measurement techniques and numerical simulations have enabled the accurate resolution of kinematics at fine spatial and temporal scales (1, 2). Active locomotion is a major component of the ecology of many plankton species and a leading contributor to their evolutionary success (3). At large scales, locomotion plays an important role in determining the spatial distribution of plankton in the environment (4). At smaller scales, it permits searching strategies and hence confers an advantageous position with respect to resources, predators, and mating opportunities (5, 6).

For small zooplankton that are around 1 mm in size, it is challenging to live in an unsteady, turbulent environment. Flow motion drives their patterns of dispersal and can redistribute organisms over large distances (7). Turbulent advection also unsettles the innate kinematics and geometrical properties of their motion (8), thereby reducing individual fitness (9). Turbulence also provides organisms with hydrodynamic signals that may be wrongly interpreted as generated by an approaching predator and which may affect their behavior and the energetic cost of swimming. It is therefore essential to know how zooplankton react to turbulence and how they have adapted to life in unsteady flow conditions.

Calanoid copepods are the most abundant metazoic zooplankton. These small organisms are particularly well suited for studying the coupling between flow motion and behavior in the plankton. They possess relatively narrow swimming capabilities, yet are capable of maintaining the distribution of their population amid strong hydrodynamic conditions (10–12). Moreover, field studies suggest that calanoid copepods react behaviorally to turbulence, which leads to the displacement of entire populations. For instance, some species actively migrate to avoid turbulent conditions at the surface of the open ocean (13) or to avoid tidal advection in estuaries (14). Many species of calanoid copepods swim by alternating periods of slow cruising motion with frequent relocation jumps. The slow forward motion derives from the creation of feeding currents accomplished by the high-frequency vibration of the cephalic appendages (15). Relocation jumps originate from the repeated beating of the swimming legs and result in sequences of high-velocity bursts leading to an intermittent motion (16). When turbulent transport dominates over slow swimming speeds, calanoid copepods drift with the flow until they perform a relocation jump (8). Since copepods can accelerate much more strongly than the flow (17), these frequent, swift movements may provide the ability to display active locomotion despite turbulent transport. However, direct evidence for behavioral response to turbulence is scarce (8), and the characteristics of individual behavior that permit population-scale features are not yet understood.

Significance

Zooplankton possess narrow swimming capabilities, yet are capable of active locomotion amid turbulence. By decoupling the relative velocity of swimming zooplankton from that of the underlying flow, we provide evidence for an active adaptation that allows these small organisms to modulate their swimming effort in response to background flow. This behavioral response results in reduced diffusion at substantial turbulence intensity. Adjusting motility provides fitness advantage because it enables zooplankton to retain the benefits of self-locomotion despite the constraints enforced by turbulence transport. Vigorous swimming and reduced diffusion oppose turbulence advection, can directly affect the dispersal of zooplankton populations, and may help these organisms to actively control their distribution in dynamic environments.

Author contributions: F.-G.M. and M.H. designed research; F.-G.M. performed research; S.S. and M.H. contributed new reagents/analytic tools; F.-G.M., I.F., and M.H. analyzed data; and F.-G.M., I.F., and M.H. wrote the paper.

The authors declare no conflict of interest.

This article is a PNAS Direct Submission.

[1]To whom correspondence should be addressed. Email: michalec@ifu.baug.ethz.ch.

This article contains supporting information online at www.pnas.org/lookup/suppl/doi:10.1073/pnas.1708888114/-/DCSupplemental.

Calanoid copepods have evolved sensitive mechanoreceptors in their prominent first antennae to detect velocity gradients created by moving predators and respond with powerful swimming strokes called escape jumps to these hydrodynamic signals. Laboratory measurements report on strong escape reactions when copepods are exposed to small, local flow velocity gradients (18, 19). Since most calanoid copepods are pelagic to epibenthic, they experience a large variety of turbulence conditions that often exceed reported threshold values for escape reactions (20). It is therefore important to understand whether copepods react to local hydrodynamic signals when exposed to turbulence and the response of these organisms to realistic flow conditions. However, to date, most studies have focused on the hydrodynamic signals that trigger escape reactions in still fluid or laminar flows, which are very different from their natural environment.

Here, we report an advance in the study of biophysical interactions in the plankton. Using four high-speed cameras, we track simultaneously and in three dimensions the motion of tracer particles and planktonic copepods swimming freely at different intensities of turbulence that are representative of their habitats. We quantify the 3D flow field around every copepod and along their trajectories, retrieve their relative velocity, and isolate a large number of jumps that otherwise would be almost indistinguishable from the underlying turbulence fluctuations. We show that copepods modulate their swimming activity in response to turbulence intensity by synchronizing their jumping frequency with the small-scale features of the flow. However, this synchronization is nonlocal in time, and the probability of jumping is independent of the instantaneous magnitude of the local hydrodynamic stresses. This behavioral response suggests that copepods integrate hydrodynamic information from the background flow over longer timescales and modulate their swimming effort accordingly. Drawing on our experimental results, we model the motion of copepods swimming in turbulence. We find that active motion enhances the diffusion of organisms at low turbulence intensity whereas it dampens diffusion at higher turbulence levels. We suggest that this previously unnoticed behavioral mechanism might help zooplankton to reduce turbulence advection under strong hydrodynamic conditions. The increase of jump frequency with turbulence intensity also provides a mechanistic explanation for the ability of planktonic copepods to control their distribution despite limited swimming capabilities. This study offers insight into the success of an ecologically important and widespread plankton group and provides a realistic model of zooplankton motion in turbulence.

Results and Discussion

Flow Parameters. The flow is forced by counterrotating disks located on the two opposite side walls of the experimental tank (see *Materials and Methods* for additional details). Relevant parameters for the flow in the measurement domain are given in Table 1. We varied the forcing such that the mean energy dissipation rate $\bar{\epsilon}$ increased from 7.7×10^{-7} m^2 s^{-3} to 1.1×10^{-4} m^2 s^{-3} and the Kolmogorov timescale τ_η decreased from 1.2 s to 0.1 s as the rotation speed of the disks increased. These values are in the upper range of average turbulence intensities measured in the open ocean under normal conditions, where $\bar{\epsilon}$ is typically on the order of 10^{-5}–10^{-4} m^2 s^{-3} a few meters below the surface (21, 22) and decreases substantially to approximately 10^{-8} m^2 s^{-3} below the mixed layer (23, 24). However, turbulence is highly intermittent in both space and time, and field studies show that it varies greatly throughout the mixed layer and the pycnocline (25). Our values are also comparable to those measured in many plankton habitats, e.g., coastal zones and estuaries where $\bar{\epsilon}$ reaches 10^{-4} m^2 s^{-3} (26, 27).

Table 1. Turbulence parameters

rpm	$\bar{\epsilon}$, m^2 s^{-3}	τ_η, s	η, mm	u, mm s^{-1}	R_λ
50	7.7×10^{-7}	1.2	1.1	3.1	41
150	5.5×10^{-6}	0.4	0.7	6.6	69
250	3.5×10^{-5}	0.2	0.4	11.1	78
350	1.1×10^{-4}	0.1	0.3	16.2	94

$\bar{\epsilon}$ is the space- and time-averaged turbulent energy dissipation rate. $\tau_\eta = (\nu/\epsilon)^{1/2}$ and $\eta = (\nu^3/\epsilon)^{1/4}$ are the Kolmogorov timescales and length scales, respectively. u is the root-mean square of the velocity fluctuations. R_λ is the Taylor Reynolds number. The velocity fluctuation is defined for each trajectory point as $u' = (u'_x + u'_y + u'_z)^{1/2}$.

Active and Advective Components of Plankton Motion. We provide in Fig. 1 the time series of the magnitude of the relative velocity of a copepod u_r and the time series of the local strain rate $(S_{ij}S_{ij})^{0.5}$, where S_{ij} is the symmetric part of the velocity gradient tensor, for three representative trajectories recorded at 350 rpm. The magnitude of the relative velocity is defined as $u_r = \|\boldsymbol{u}_c - \boldsymbol{u}_f\|$, where $\boldsymbol{u}_c$ is the copepod velocity in laboratory coordinates and $\boldsymbol{u}_f$ is the local instantaneous flow velocity. Because the swimming velocities that derive from the creation of feeding currents are very low, on the order of a few millimeters per second in *Eurytemora affinis*, they do not contribute significantly to locomotion when turbulence intensities are significant, and copepods approximately drift with the flow unless executing a relocation jump (17). Therefore, the motion of copepods swimming in turbulence consists of an active component, i.e., their relocation jumps, and an advective component that is due to transport by the flow. Fig. 1 shows that while these jumps display various amplitudes, most often they reach peak velocities of a few tens of millimeters per second. Copepods sometimes perform more powerful jumps, but these jumps are far less frequent: Jumps that reach velocities in excess of 100 mm s^{-1} represent 0.3% of the total number of jumps at 350 rpm and less than 0.1% in calm water. Jumps occur either in isolation (Fig. 1*A*) or in sequence (Fig. 1*B*). Surprisingly, it appears that jumps do not directly result from a local turbulence event: Fluctuations in turbulence intensity are frequent but do not trigger escape reactions (Fig. 1*B*) and similarly, even powerful jumps typically occur in the absence of a strong hydrodynamic signal (Fig. 1*C*).

Turbulence Increases Jump Frequency. We quantify the effort associated with active swimming by considering the instantaneous power per unit mass $P(t) = \mathbf{a}(t) \cdot \mathbf{u}(t)$, where $\mathbf{a}(t)$ is the acceleration vector of a particle (i.e., living copepod or flow tracer) at time t and $\mathbf{u}(t)$ is its velocity vector (Fig. 2). We use the relative velocity and acceleration for living copepods to quantify the power of the active component of the motion and the absolute velocity and acceleration for tracer particles. Fig. 2 shows that $P_{copepods}$ is larger than $P_{tracers}$ by an order of magnitude. This was expected, because at these intensities of turbulence, copepods can accelerate much more strongly than the flow (8). We also observe a more than twofold increase in $P_{copepods}$ from calm water to 350 rpm, which indicates that copepods increase their swimming effort as turbulence increases. Because active locomotion in turbulence occurs through jumps (17), this higher swimming effort suggests a more energetic jumping behavior driven by higher turbulence intensities.

To confirm this observation, we probe the statistical properties of jumps in more detail to look for signatures of interaction between turbulence and jumps. Since dissipation and stress are directly related in turbulence, we use the values of the local energy dissipation rate ϵ measured along copepod trajectories as a proxy for the hydrodynamic stresses exerted on an organism by the flow. For different thresholds ϵ_{cr} that span several orders of magnitude, we measure the separation times between consecutive threshold

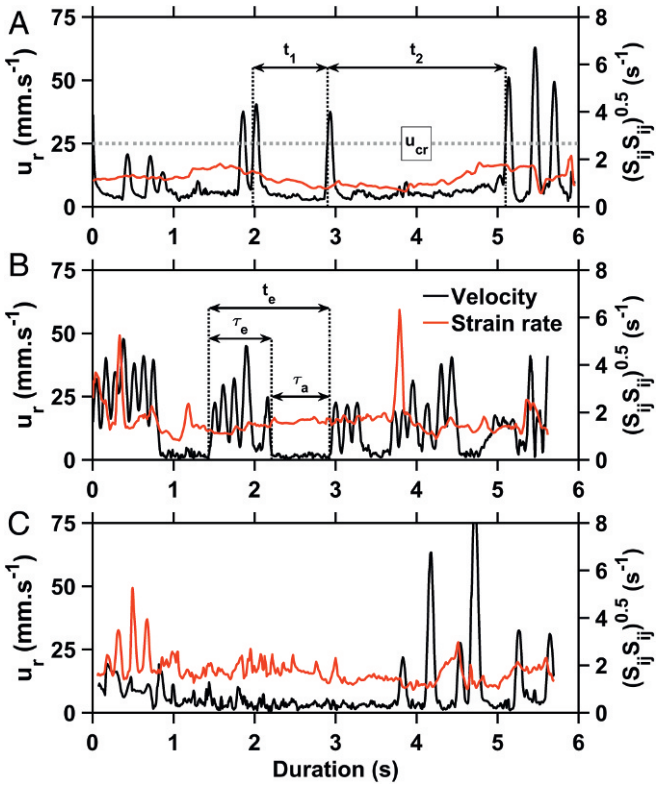

Fig. 1. Times series of the magnitude of the relative velocity of a copepod u_r (black) and of the local strain rate $(S_{ij}S_{ij})^{0.5}$ along its trajectory (red) for three representative trajectories recorded at 350 rpm. *A* illustrates the separation times t_1 and t_2 between consecutive threshold up-crossing events, for a given velocity threshold u_{cr} (indicated by a gray dashed line) of the copepod relative velocity. Separation times between consecutive threshold up-crossing events of the local dissipation rate are defined analogously using a dissipation threshold ϵ_{cr}. The inverse of the mean separation time gives the frequency at which u or ϵ exceeds a critical value. *B* illustrates the waiting time t_e between two effective jumps, the duration τ_e of an effective jump, and the duration τ_a of an advection phase. *C* shows a cluster of turbulent events and two powerful jumps that occur in the absence of a strong hydrodynamic trigger.

up-crossing events along the trajectories of copepods (28). The frequency of turbulence events that are strong enough to cross a given threshold is then given by the inverse of the mean separation time. We conduct the same analysis using the relative velocity u of the copepods. The frequency of jumps that are powerful enough to cross a critical velocity value u_{cr} is given by the mean separation time between consecutive up-crossing events (Fig. 1*A*). This approach enables us to evidence any relationship between the mean frequency of dissipation bursts and that of relocation jumps. Considering many thresholds ϵ_{cr} and u_{cr} allows us to capture the large variability in the local dissipation rate and in jump amplitude. Fig. 3 shows that jump frequency increases with turbulence intensity. It also shows that the frequency of turbulence events parallels that of jumps very well; that is, for the range of turbulence intensities tested here, the turbulent properties of the background flow seem to drive the jumping behavior of copepods. The increase in jump frequency is substantial: For instance, considering a velocity threshold $u_{cr} = 30$ mm s^{-1}, copepods jump on average 19 times per minute in calm water and 60 times per minute at 350 rpm.

Synchronization Without Local Correlation. In our measurements, copepods often experience strain rates that are higher than the threshold, previously estimated between 2 s^{-1} and 3 s^{-1}, needed to trigger escape reactions in *E. affinis* swimming in calm water (30–32). However, we show in Fig. 4 that the probability density functions of the local dissipation rate at the onset of jumps and during advection in turbulence overlap with each other, which indicates that local events of strong turbulence usually do not trigger escape jumps, even when turbulence quantities are well above reported threshold values. We observe a similar overlap when plotting the shear stress, the normal stress, the inertial drag stress, and the vorticity (Fig. S1). We note that the inertial drag stress is much larger than the shear and normal stresses and yet it does not elicit escape responses, which is expected because the inertial drag stress causes a uniform velocity difference along the antennules, and thus it creates a signal which is similar to that created by the motion of the copepod (18).

We confirm this surprising observation by considering the jump angle, that is, the angle between the direction of motion at the onset of jump and the jump displacement vector. Previous studies report that calanoid copepods direct their jumps away from the source of the hydrodynamical disturbance (32–34). In our measurements, however, the jump direction is predominantly directed along the direction of motion and does not change with turbulence intensity, which suggests that, despite being exposed to strong and local turbulence perturbations, copepods maintain the directional properties of the innate jumping behavior that they display in the absence of hydrodynamical signals (Fig. S2). Since we isolated a large number of jumps (8,156 jumps in calm water, 7,643 jumps at 50 rpm, 5,345 jumps at 150 rpm, 5,671 jumps at 250 rpm, and 20,190 jumps at 350 rpm), we can estimate statistically reliable mean values and variances. We find that jump amplitude, computed from the relative velocity of the organisms, increases only slightly, from 13.7 ± 11.3 mm s^{-1} in calm water to 18.4 ± 15.4 mm s^{-1} at 350 rpm, and that jump duration remains remarkably constant at 200 ± 60 ms under all tested flow conditions. Since escape reactions in calanoid copepods are usually much more powerful, e.g., 150 mm s^{-1} or more in *E. affinis* (8, 32) and also shorter than relocation jumps (35, 36), these results suggest that these organisms, when swimming in quasi-homogeneous and isotropic turbulence, do not in most cases perform escape jumps when sensing localized turbulence events. This observation is consistent with a recent study on the behavior of *Acartia tonsa* swimming freely in a recirculating channel (37). The authors observed powerful escape jumps in the laminar region directly upstream of a cylinder in response to strain rates as low as 0.25 s^{-1}, but not in its turbulent wake, despite fluctuating strain rates up to 20 s^{-1}. It also agrees with the previous finding that *A. tonsa*, albeit very

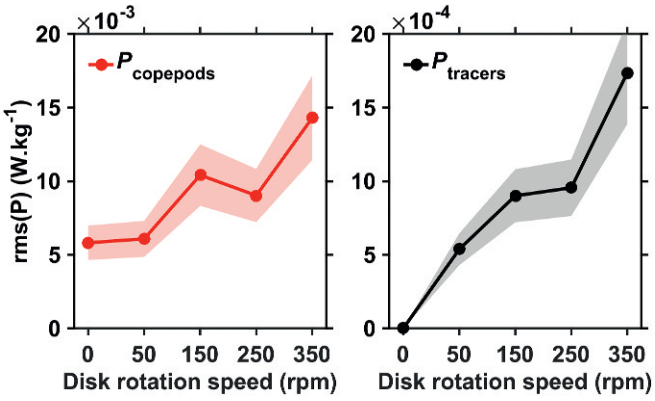

Fig. 2. Root-mean square of the instantaneous power per unit mass *P* for living copepods (red) and tracer particles (black). $P_{copepods}$ is larger than $P_{tracers}$ by an order of magnitude. The shaded areas show the measurement uncertainty due to the relative error (estimated at about 20%) in the Lagrangian acceleration (29).

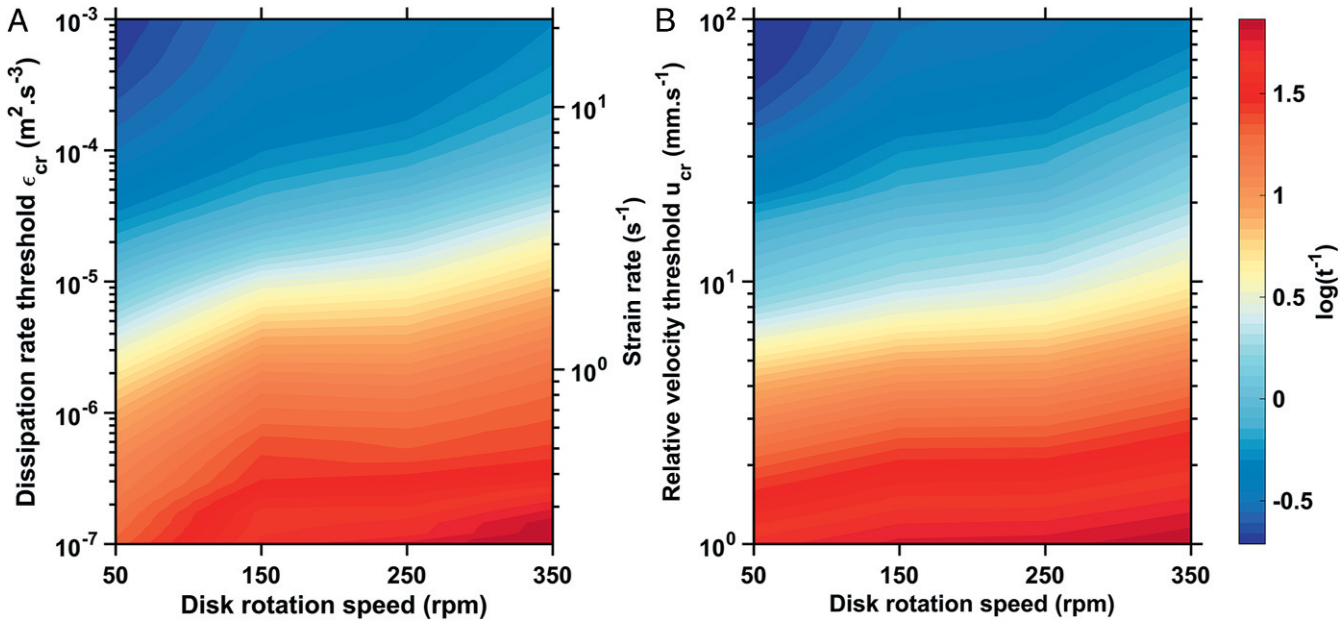

Fig. 3. (*A*) The evolution of $\log(t^{-1})$, where t is the mean separation time between consecutive threshold up-crossing events, with the disk rotation speed, for different thresholds ϵ_{cr} of the energy dissipation rate. The corresponding strain rate is indicated as a reference. (*B*) The evolution of $\log(t^{-1})$ with the disk rotation speed, for different thresholds u_{cr} of the copepod relative velocity.

sensitive to hydrodynamic signals, does not perform unnecessary escape reactions when swimming in a turbulent flow (38). It would appear then that copepods do not react to the turbulence properties of the background flow the same as they react to localized hydrodynamic disturbances of comparable intensities in a still environment.

We find further support for this conclusion by studying the clustering properties of jumps and of hydrodynamic signals and their correlation in time. As shown in Fig. 1, relocation jumps sometimes occur in isolation, but most often cluster. These clusters are separated by periods of slow swimming in calm water and by periods of advection by the flow in turbulence. We therefore consider the telegraph approximation of dissipation rate and copepod relative velocity time series (39). This approximation is generated from the measured signal by replacing each value by zero or one, depending on whether the signal magnitude exceeds a given threshold. This approach ignores variations in amplitude and retains the threshold-crossing information only. For different thresholds ϵ_{cr} and u_{cr}, we consider the exponent α that governs the scaling of the root-mean square of the running density fluctuations $\delta n_\tau = n_\tau - \langle n_\tau \rangle$, where n_τ is the average density of threshold-crossing events over a time window τ, and $\langle n_\tau \rangle$ denotes an average over long times. This exponent provides a quantitative measure of the clustering tendency of a signal. Previous studies report that $\alpha = 0.5$ for white noise and that $\alpha < 0.5$ in the dissipative and inertial range of turbulence (39). In our measurements, α_ϵ ranges from 0.39 ± 0.03 at 50 rpm to 0.42 ± 0.03 at 350 rpm (Fig. S3), which agrees well with previous observations on the clustering properties of fine-scale dissipation signals. We show in Fig. S3 that α_u ranges from 0.39 ± 0.04 in calm water to 0.40 ± 0.04 at 350 rpm, which confirms that jumps are not randomly distributed in time, but instead tend to cluster. Two questions arise: Are clusters of jumps triggered by clusters of turbulent stress events? And can we evidence a time lag between a cluster of turbulent events and the subsequent cluster of jumps, assuming that the behavioral response has some delay with respect to the trigger? We thus consider the correlation between u, the magnitude of the relative velocity of the copepods, and ϵ, the local dissipation rate along their trajectories. We compute $C(t) = \langle \rho(u_i, \epsilon_{i-t}) \rangle$ for different time increments δt and for values of ϵ averaged over a time window τ. Computing $C(t)$ for different τ allows us to assess and compare the influence of turbulent events that occur over different timescales. Fig. S3, *Inset* shows the lack of local correlation between u and ϵ for δt up to 2 s and for τ ranging from 0.1 s to 2 s, which confirms that copepods integrate hydrodynamic information over long timescales. These results show that not only do copepods not respond to single, localized turbulence bursts when swimming in turbulence, but also they do not jump upon sensing a cluster of turbulence events.

We expand our analysis by testing for a possible influence of mating behavior on jump frequency. *E. affinis* females release a trail of pheromones that males detect and follow (40). In species that use pheromones to increase mating probabilities, males modify their motion upon detection of the chemical signals

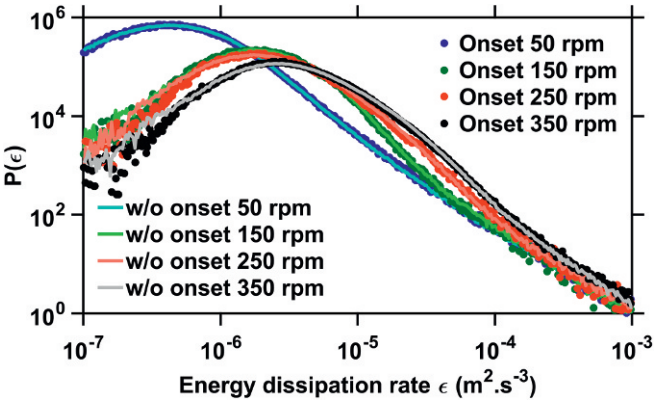

Fig. 4. Probability density functions of the local energy dissipation rate ϵ measured at the onset of jumps (solid circles) and along copepod trajectories without including jump onset positions (solid lines) at 50 rpm (dark and light blue), 150 rpm (dark and light green), 250 rpm (dark and light red), and 350 rpm (black and gray).

and orient their approach to females. Jumps may occur at different stages of the approach. They enable males to race up the pheromone trail, to follow a broken trail, and to leap toward the female during the last step of the approach (41, 42). We repeat our measurements using single adult copepods (males or females) in calm water and at 350 rpm and record for long durations to obtain sufficient statistics (several hundred jumps for each case). We show in Fig. S4 that the jump frequency increases twofold both for mixed genders and for single males or single females, which rules out the presence of nearby organisms as a cause of increased jump frequency.

A Model for Plankton Motion in Turbulence. We explore further the ecological implication of our results by modeling the motion of zooplankton swimming in turbulence. Because calanoid copepods accelerate on a timescale that is much shorter than both the Kolmogorov timescale τ_η and the Stokes time of a copepod (19, 35), we consider jumps as instantaneous acceleration events that provide copepods with a finite velocity $\boldsymbol{\psi}$ with respect to the underlying flow. Immediately after this sudden acceleration, a copepod swimming in turbulence moves with a velocity $\boldsymbol{u}+\boldsymbol{\psi}$, where $\boldsymbol{u}$ is the velocity of the flow local to the organism. Galilean invariance implies that if the size of the organism is much smaller than the viscous scale of the flow, then the statistics of $\boldsymbol{\psi}$ are independent of the intensity of turbulence. Because in our measurements the viscous scale is smaller, but within the same order of magnitude, than the size of a copepod, the statistics of $\boldsymbol{\psi}$ should depend only weakly on the strength of turbulence. Indeed, the average jump amplitude is comparable across turbulence intensities. We thus consider the velocity $\boldsymbol{\psi}$ gained during an acceleration event as a random vector drawn from a fixed distribution $P(\boldsymbol{\psi})$ that is independent of $\boldsymbol{u}$. Observing copepod velocity time series reveals that jumps often occur in sequence (Fig. 1). We therefore consider that two jumps cluster when their separation time is less than twice the mean jump duration. We refer to these jumps as clustering jumps. Our measurements indicate that (*i*) most jumps cluster (Fig. S5*A*); (*ii*) the mean waiting time $\langle t_{cj}\rangle$ between jumps within the same cluster (that is, between consecutive clustering jumps) is comparable to their mean duration $\langle \tau_{cj}\rangle$, which shows that the duration of the advection phase between the end of the coasting phase and the onset of the next clustering jump is negligible (Fig. S5*B*); (*iii*) the duration of clustering jumps remains constant at 180 ± 5 ms across turbulence intensities; and (*iv*) the waiting time between clustering jumps does not depend on turbulence intensity (Fig. S5*B*). This allows us to consider in our model both isolated jumps and clusters of jumps as single effective jumps. The duration τ_e of an effective jump is the total duration of the isolated jump or the total duration of the cluster, and the velocity is the total displacement vector $(\delta\boldsymbol{x})_e$ divided by τ_e. We note that the waiting time $\langle t_e\rangle$ between effective jumps decreases as turbulence intensity increases, in agreement with the increase in jump frequency shown in Fig. 3. Our results also show that $\langle\tau_e\rangle$ remains approximately constant at 390 ± 20 ms across turbulence intensities and that the mean waiting time $\langle t_e\rangle$ between effective jumps is much larger than $\langle\tau_e\rangle$ (Fig. S5*B*). We therefore define the motion of a copepod swimming in turbulence as the sum of the contributions of flow transport and jump events,

$$\frac{d\boldsymbol{x}}{dt}=\boldsymbol{u}(t,\boldsymbol{x}(t))+\sum_i \boldsymbol{\psi}(t-t_i), \qquad [1]$$

where $\boldsymbol{x}(t)$ is the copepod coordinates at time t, t_i is the time onset of the ith effective jump, and $\boldsymbol{\psi}(t)$ is the velocity of the copepod during an effective jump in the absence of turbulence. The velocity $\boldsymbol{\psi}$ is a vector function that obeys $\boldsymbol{\psi}(t<0)=0$ and has a finite support of random duration whose average is equal to $\langle\tau_e\rangle$. Integrating for the displacement $\delta\boldsymbol{x}(t)=\boldsymbol{x}(t)-\boldsymbol{x}(0)$ gives

$$\delta\boldsymbol{x}(t)=\int_0^t \boldsymbol{u}(t',\boldsymbol{x}(t'))\,dt'+\sum_i \delta\boldsymbol{x}_i, \qquad [2]$$

where $\delta\boldsymbol{x}_i$ is the displacement due to the drift caused by the ith effective jump:

$$\delta\boldsymbol{x}_i=\int_0^t \boldsymbol{\psi}(t'-t_i)\,dt'. \qquad [3]$$

By considering the mean-square displacement $\langle(\delta x(t))^2\rangle$ in Eq. **2**, we obtain

$$\langle(\delta x(t))^2\rangle=2t\int_0^\infty \langle\boldsymbol{u}(0),\boldsymbol{x}(0)\cdot\boldsymbol{u}(t',\boldsymbol{x}(t'))\rangle\,dt' + \frac{t\langle(\delta x)^2\rangle_e}{t_e}(1+2c_1+2c_2+\ldots), \qquad [4]$$

where t_e is the mean waiting time between consecutive effective jumps, and $\langle(\delta x)^2\rangle_e$ is the mean-square displacement during an effective jump. We have introduced the correlation coefficients of the displacements during the ith and $i+k$th effective jumps:

$$c_k=\frac{\langle\delta\boldsymbol{x}_i\cdot\delta\boldsymbol{x}_{i+1}\rangle}{\langle(\delta x)^2\rangle_e}. \qquad [5]$$

Our results indicate that these correlation coefficients c_k decay rapidly as the separation k grows. From Eq. **4** we obtain the diffusion coefficient D_L of living copepods swimming in turbulence:

$$D_L=\frac{1}{3}\int_0^\infty \langle\boldsymbol{u}(0),\boldsymbol{x}(0)\cdot\boldsymbol{u}(t',\boldsymbol{x}(t'))\rangle\,dt' + \frac{\langle(\delta x)^2\rangle_e}{6t_e}(1+2c_1+2c_2+\ldots). \qquad [6]$$

We note here that while the first term in the right-hand side of Eq. **6** corresponds to Taylor diffusion in the case of tracer particles, it also accounts for the presence of jumps in the case of living copepods. Indeed, when considered in the reference frame of a moving copepod, the correlation time of turbulence decreases much faster than the integral timescale of the flow (Fig. S5*C*). We compare the diffusion coefficients predicted by our model with those determined from the Lagrangian velocity autocorrelation function of copepods swimming in turbulence, after removing the weak mean flow present in the investigation volume and hence assuming that $\langle[\boldsymbol{v}(t)-\langle\boldsymbol{u}(x(t))\rangle]\cdot[\boldsymbol{v}(0)-\langle\boldsymbol{u}(x(0))\rangle]\rangle$ is a good approximation to $\langle\boldsymbol{v}(t)\cdot\boldsymbol{v}(0)\rangle$ that would hold in homogeneous isotropic turbulence with zero mean flow. Fig. 5 shows that the diffusion coefficients predicted by the model agree very well

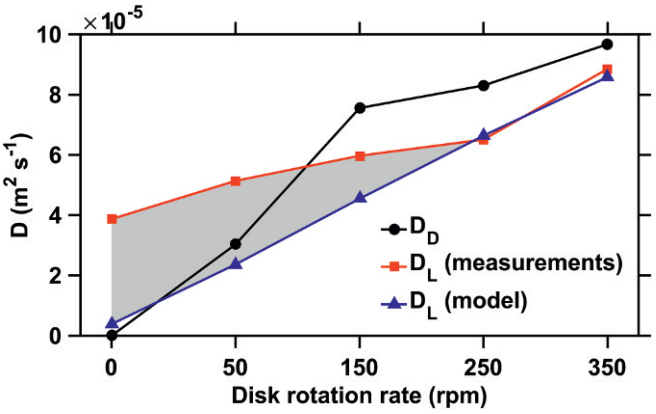

Fig. 5. Diffusion coefficients of dead copepods (black circles) and living copepods (red squares) from particle-tracking measurements and diffusion coefficients of living copepods estimated by the model (blue triangles). The shaded area indicates the contribution of cruising motion to D_L.

with our experimental results when the intensity of turbulence is substantial (250 rpm and 350 rpm). The discrepancy between the measured and estimated coefficients grows as turbulence intensity decreases because of an increasing contribution of cruising motion on diffusion at low turbulence levels and also because Galilean invariance can no longer apply as the viscous scale of turbulence becomes very close to the size of a copepod. In calm water, the contribution of cruising motion is maximal, and jumps contribute only marginally to diffusion. This observation is not surprising, because in still water copepods jump much less than in turbulence (Fig. 3). The contribution of cruising behavior to diffusion weakens as turbulence grows. At substantial turbulence intensities, the diffusion coefficient of living copepods remains lower than that of inert particles (Fig. 5), which indicates that jumps do not enhance diffusion, but instead oppose turbulence advection. Hence, vigorous jumping enables copepods to diffuse less than nonmotile particles when turbulence intensities are substantial. This surprising observation suggests that copepods have evolved a behavioral mechanism that aims at maintaining the innate diffusive properties of their motion despite turbulence advection, at least up to a level where flow transport overwhelms their swimming capabilities.

It is important to note that the diffusion coefficient of living copepods can be estimated as $D_L = \kappa D_D(\tau_L/\tau_D) + D_e$, where the contribution of effective jumps is given by $D_e = (\delta x)^2/(6t_e)\times (1 + 2c_1 + 2c_2 + \ldots)$, D_D is the Taylor diffusion coefficient of tracer particles, τ_L and τ_D are the correlation times of turbulence in the reference frame of a living and a dead copepod, respectively, and κ is a constant of order one. It can be readily seen that because jumping more often simultaneously decreases τ_L and increases D_e, the resulting net effect of the behavioral response on D_L is indefinite and depends on flow transport through D_D and τ_D. Due to its limited size and Galilean invariance, a copepod swimming in turbulence is unable to perceive τ_D, which is a large-scale quantity of the flow. It can, however, perceive small-scale velocity gradients (19). Our results show that the small-scale turbulent features of the background flow drive the jumping frequency of copepods. We therefore suggest that the selection of this behavioral trait was driven by the evolutionary advantage it provides: Swimming vigorously upon detecting small-scale hydrodynamic signals enhances fitness because it gives zooplankton the capability to respond to the larger features of turbulent flow.

A New Perspective on Biophysical Interactions. Our results indicate that copepods have the capability to integrate sensory inputs from the background flow over long times and adjust their swimming effort accordingly. They reveal the existence of an innate mechanism for active locomotion amid turbulence and mirror recent studies that report on the effects of ambient flow on the swimming behavior of other marine organisms such as sea urchin larvae (43) or oyster larvae (44, 45). For instance, oyster larvae swim more forcefully and direct their swimming downward at high turbulence intensity, and these fast descents enable them to rapidly approach the seabed in the strong turbulence associated with coastal habitats (46). The active adaptation to turbulence identified in our measurements may enhance fitness via several mechanisms. Zooplankton may couple vigorous jumping behavior with a bias in their direction of motion to reach specific regions in the water column despite the constraints enforced by flow transport in large-scale turbulent environments (47). Calanoid copepods are known to migrate vertically and to accumulate, a mechanism that produces patchiness along tidal fronts (12) and phytoplankton layers (48). In the open ocean, studies report that certain species actively migrate over tens of meters toward calmer environments below the turbulent mixed layer (13, 49, 50) to maximize their fitness with respect to foraging efficiency and predation pressure (51). In tide-dominated estuaries, copepods migrate vertically to prevent tidal flushing (11). For instance, *E. affinis* migrates to the bottom layer, both at ebb tide and during the late rising tide, and can therefore maintain its population despite very high dissipation rates and mean current speed beyond 2 m s^{-1} (14, 52). The existence of frequent relocation jumps of substantial velocity in a motion that is otherwise determined by turbulent transport allows for the possibility of reorientations and active locomotion, that is, to break down the directional restriction imposed by turbulent transport and to transition from being weakly inertial particles to being able of self-locomotion in turbulent flows. Support for this hypothesis comes from observations that adults and late-stage copepodites, which have better jumping abilities, migrate to the bottom layer, both at ebb tide and during the late rising tide, whereas nauplii are transported as passive particles in the turbidity maximum zone (14). Because individual diffusion directly affects the dispersal of zooplankton populations, lowering diffusion via vigorous jumping may also provide zooplankton with the capability to efficiently reduce turbulence advection and hence to maintain the core of their population under varying hydrodynamic conditions (11, 12). We suggest that a reduced diffusion may also provide advantages at smaller scales: Opposing turbulence advection may enable copepods to maintain their innate swimming patterns, that are shaped to efficiently explore volumes at small scales (6), and hence to retain fitness in dynamic environments.

One interesting question is whether turbulence-induced vigorous swimming generates higher predation risk. A previous study indicates that the flow field generated by a repositioning jump quickly evolves into two counterrotating viscous vortex rings that are of similar intensity, one in the wake and one around the body of the copepod (53). The authors conclude that this near symmetrical flow may help copepods to hide from rheotactic predators, because it contains no information about the position of the copepod within the flow structure (16). These repositioning jumps quickly attenuate both spatially and temporally and give rise to vorticity values ranging up to 10 s^{-1} and to flow velocities that can reach 10 mm s^{-1} (15). These values are comparable to those, created by turbulence, that we observe in our measurements (Table 1). Our results also indicate a remarkably similar clustering exponent for turbulence signals and jump events. We therefore suggest that performing frequent relocation jumps in turbulent flow does not necessarily expose copepods to a higher risk of predation by rheotactic predators, because the hydrodynamic signals that copepods generate while jumping blend with the small-scale structure of turbulence, both spatially and temporally. Finally, in our measurements, copepods did not react to strain rates that are comparable to those measured in the bow wave of a fish during the approach phase of the capture and the initial phase of the feeding strike (54). Our results therefore suggest that copepods do not wrongly interpret the hydrodynamic signals associated with turbulence generated by an approaching predator. Exploring this feature in future work may lead to important insights into the interplay of background flow, organism motility, and predation in the zooplankton community.

Conclusion

Recent research—mainly conducted with bacteria and phytoplankton—has demonstrated that the interactions of turbulence with plankton behavior can drive many important ecological processes and shape the macroscopic features of marine ecosystems (2, 55, 56). Our knowledge is much more limited in zooplankton. Their ability to perform active motion amid ambient currents has been demonstrated in the ocean (4, 12), but direct evidence for behavioral response to turbulence is scarce, and the characteristics of individual behavior that permit population-scale features are not yet understood. Through simultaneous, 3D measurements of flow motion and copepod swimming behavior, we highlight several unexpected results with respect to their

behavior in turbulence. We show that when exposed to substantial intensities of turbulence, copepods respond with a rapid increase in the effort allocated to swimming, via more frequent relocation jumps whose frequency synchronizes with that of small-scale turbulence, while maintaining many of the innate characteristics of their motion (jump amplitude, duration, clustering properties, and orientation). Our model and measurements indicate that active motion enhances diffusion at low turbulence intensity, whereas it reduces diffusion at higher turbulence levels. This active behavioral adaptation carries strong fitness advantages because it enables these small organisms to retain the benefits of self-locomotion under varying flow conditions. It gives them the capability to maintain the diffusive properties of their motion, to control their distribution despite strong hydrodynamics, and to regulate the dispersal of their population—a behavioral trait that provides selective advantage even when the difference in diffusivity is small (57). Since encounter processes and range expansion depend on diffusion coefficients, our study also has important implications for the modeling of the dynamics and distribution of planktonic organisms.

Materials and Methods

Copepod and Algae Cultures. *E. affinis* individuals were obtained from laboratory cultures that originate from copepods sampled in September 2014 from the oligohaline zone of the Seine Estuary. Copepods were cultured in aerated 20-L to 300-L containers, at a temperature of 18 °C, at salinity 15 (seawater from the English Channel adjusted to salinity with deionized water), and under a fluorescent light:dark cycle of 12L:12D. They were fed with the microalgae *Rhodomonas baltica* cultured in autoclaved seawater at salinity 30, in Conway medium, under a 12L:12D light cycle, and at a temperature of 18 °C.

Experimental Setup. We conducted 3D particle-tracking velocimetry measurements, using four synchronized Mikrotron EoSens cameras (Fig. S6). Three cameras were equipped with red band-pass filters and recorded the motion of fluorescent tracer particles. The fourth camera was equipped with a green band-pass filter and mounted in front of an image splitter, which is an optical arrangement that allows stereoscopic imaging using one single camera. This camera recorded the motion of copepods. The cameras were fitted with Nikon 60-mm lenses and recorded on two DVR Express Core 2 devices (IO Industries) at 200 Hz (fast enough to resolve the acceleration of the copepods) and at a resolution of 1,280 × 1,024 pixels. Illumination was provided by a pulsed laser (527 nm, pulse energy of 60 mJ). We conducted measurements in a 27-cm (width) × 18-cm (depth) × 17-cm (height) glass tank containing a forcing device creating quasi-homogeneous and isotropic turbulence (58). The device is driven by a servomotor and is composed of two arrays of four counterrotating disks located on the lateral sides of the aquarium. The disks are 40 mm in diameter and smooth to prevent mechanical damage to the copepods.

Recording Conditions. Simultaneous measurements of flow motion and copepod swimming behavior were conducted in a 6-cm × 6-cm × 3-cm investigation volume centered in the middle of the aquarium. To record the motion of the flow, we used fluorescent tracer particles with a density of 1 g cm^{-3} and a mean diameter $d_p = 69$ μm. The Stokes number of these particles is defined as $S = (d_p/\eta)^2/12\beta$, where $\beta = 3\rho_f/(2\rho_p + \rho_f)$ is the modified density ratio that takes into account the added mass effect, η is the Kolmogorov length scale, and ρ_p and ρ_f are the particle and fluid densities, respectively. In our measurements, S ranges from 3.25×10^{-4} to 4.4×10^{-3}, indicating that these particles behave as passive tracers. They were also much smaller than η (Table 1). The average seeding density was 17 ± 8 particles per cubic centimeter (Fig. S7). We checked copepods for integrity under a microscope and selected healthy and well-fed individuals. For each measurement, we transferred 300 adult copepods (150 males and 150 females) into the experimental aquarium and allowed them to acclimate for 5 min. We recorded the motion of copepods and tracer particles in still water and at different disk rotation rates: 50 rpm, 150 rpm, 250 rpm, and 350 rpm (Table S1). Each sequence was preceded by a 1-min period for the flow to develop fully and for the copepods to acclimate to the new turbulence intensity. Water temperature increased from 18 °C to 19 °C at the end of the recording. The number density of copepods used in our measurements (∼150 individuals per liter) is low enough to reduce ambiguities in the recognition and stereo-matching of individual particles, which allows the reconstruction of long trajectories, and high enough to observe many copepods in the investigation volume (Fig. S8*A*). Moreover, this density reflects the values observed in estuaries, where the density of *E. affinis* can reach 700 individuals per liter (59). We conducted the same measurements using dead copepods to account for the effects of particle size and density (60).

Particle Tracking and Trajectory Processing. We calibrated the cameras, using a calibration plate on which reference points of known coordinates are evenly distributed along the vertical and horizontal directions, and performed an additional dynamic calibration based on the images of moving particles (61). The plate was imaged at four different positions, and the calibration was conducted using a virtual 3D object after combining the orientation data obtained during each single-plane calibration. Knowing the camera intrinsic and extrinsic parameters, we established correspondences between particle image coordinates and derived the 3D positions of the moving particles by forward intersection (62, 63). To express the coordinates of the copepods in the reference frame of the tracer particles, we used an iterative closest-point algorithm and obtained the 3D rigid transformation that aligned the two coordinate systems. We processed the image sequences and tracked particles and copepods, using an algorithm based on image and object space information (64). We glued segments belonging to the same copepod trajectory, using a spatiotemporal matching assignment (8). Copepod and tracer trajectories were smoothed with a third-order polynomial filter to improve the measurement of velocity and acceleration, which were directly estimated from the coefficients of the polynomial.

Flow Parameters. Spatial and temporal velocity derivatives were linearly interpolated for each tracer trajectory point, using weighted contributions from nearby tracers (65). At each time step, we obtained the velocity gradient tensor at the location of every tracer particle in the investigation domain. The local energy dissipation rate $\epsilon = 2\nu S_{ij}S_{ij}$, where ν is the fluid kinematic viscosity and S_{ij} the rate of strain tensor, was directly obtained for each tracer trajectory point from the measured velocity gradient tensor (29). Flow velocity, vorticity, and energy dissipation rate were interpolated at the position of copepods, using the information from the neighboring tracers and via quadratic inverse distance weighting. Neighboring tracers were defined as tracers found within a sphere of radius of 5 mm centered at the location of the copepod (Fig. S8*B*). Although this radius is larger than η, the velocity gradient tensor was resolved with sufficient accuracy: We obtained a relative error of 8% for S_{ij}, using kinematic checks based on the acceleration and on the incompressibility of the velocity field (29). We estimated the space- and time-averaged energy dissipation rate $\bar{\epsilon}$ in the investigation volume from the relation $\langle \delta_r \boldsymbol{u} \cdot \delta_r \boldsymbol{a} \rangle \approx -2\bar{\epsilon}$, where $\langle \delta_r \boldsymbol{u} \cdot \delta_r \boldsymbol{a} \rangle$ is the velocity-acceleration structure function and δ_r denotes the Eulerian spatial increment of a given quantity (66). This estimate was compared with the relation $\bar{\epsilon} \simeq C_\epsilon u_{rms}^3/L$, where C_ϵ is the dissipation rate coefficient, u_{rms} is the root-mean square of the velocity fluctuations, and L is the integral length scale, estimated for each experimental condition via the Eulerian velocity autocorrelation function. Both methods yielded comparable results. The correlation length l of the velocity gradients from a dimensional estimate is the Kolmogorov length scale $\eta = (\nu^3/\epsilon)^{1/4}$. It is important to note that finer considerations via direct numerical simulations give $l = \beta\eta$, where $\beta\eta$ is the exponent of the spectrum decay in Fourier space (67). This exponent can be substantial (approximately 5 at our turbulence intensities), which supports the assumption of Galilean invariance in our model.

Estimation of Hydrodynamic Stresses. We estimated the hydrodynamic stress due to velocity gradients local to the copepods as $\sigma_{shear} = (\rho\mu\epsilon)^{0.5}$, where ρ is the fluid density, μ the fluid dynamic viscosity, and ϵ the local energy dissipation rate at the location of the organism (68). The mass density of calanoid copepods is generally slightly higher than that of water, and in our measurements copepods were slightly bigger than η. Their Stokes number is thus significantly larger than that of tracer particles and can be estimated between 7×10^{-2} and 0.9, assuming a density of 1.03 g cm^{-3} and a body size of 1 mm (69). Since their Stokes number is not very small, copepods also experience inertial stresses. First, they experience a normal stress due to a finite velocity difference across the size of their body, which we estimated as $\sigma_{normal} = \rho(\epsilon d)^{2/3}$, where $d = 1$ mm is the average size of a copepod. Additionally, organisms also experience a drag stress. One component of the drag stress comes from their own motility. The second component is due to inertia, which causes their trajectories to deviate from the fluid streamlines. We estimated the inertial drag stress from the drift velocity due to inertia as $\boldsymbol{u}_d = \boldsymbol{a}\tau_p$, where $\boldsymbol{a}$ is the acceleration of the fluid local to the organism and τ_p is the particle relaxation time. This approach allows

us to quantify the drag stress due to inertia independently of the active component of the motion. This formula strictly applies only for particle size smaller than η but we assume that it is still valid as an order of magnitude estimate for copepods because d is not much larger than η. The relaxation time is given by $\tau_p = 2d^2/9\nu \times [3\rho_f/(2\rho_c + \rho_f)]^{-1}$, where ρ_c and ρ_f are the copepod and fluid densities, respectively. The inertial drag stress is then estimated as $\sigma_{drag} = 3\mu||\boldsymbol{u}_d||d^{-1}$.

ACKNOWLEDGMENTS. We thank the members of the group of S.S. for providing copepods and algae and the Communauté d'Agglomération du Boulonnais for supporting the implementation of a copepod-rearing pilot project. This work was supported by Swiss National Science Foundation Grant 144645 and by Swiss Federal Institute of Technology Zurich Grant 2914-1. We acknowledge support from Groupement d'Intérêt Public Seine-Aval. This work is a contribution to the bilateral agreement between ETH Zurich and Lille University.

1. Ardeshiri H, et al. (2016) Lagrangian model of copepod dynamics: Clustering by escape jumps in turbulence. *Phys Rev E* 93:043117.
2. Sengupta A, Carrara F, Stocker R (2017) Phytoplankton can actively diversify their migration strategy in response to turbulent cues. *Nature* 543:555–558.
3. Bartumeus F, Peters F, Pueyo S, Marrasé C, Catalan J (2003) Helical Lévy walks: Adjusting searching statistics to resource availability in microzooplankton. *Proc Natl Acad Sci USA* 100:12771–12775.
4. McManus MA, Woodson CB (2012) Plankton distribution and ocean dispersal. *J Exp Biol* 215:1008–1016.
5. Kiørboe T, Jiang H (2013) To eat and not be eaten: Optimal foraging behaviour in suspension feeding copepods. *J R Soc Interface* 10:20120693.
6. Bianco G, Mariani P, Visser AW, Mazzocchi MG, Pigolotti S (2014) Analysis of self-overlap reveals trade-offs in plankton swimming trajectories. *J R Soc Interface* 11:20140164.
7. Siegel DA, Kinlan BP, Gaylord B, Gaines SD (2003) Lagrangian descriptions of marine larval dispersion. *Mar Ecol Prog Ser* 260:83–96.
8. Michalec FG, Souissi S, Holzner M (2015) Turbulence triggers vigorous swimming but hinders motion strategy in planktonic copepods. *J R Soc Interface* 12:20150158.
9. Visser AW (2007) Motility of zooplankton: Fitness, foraging and predation. *J Plankton Res* 29:447–461.
10. Haury LR, Yamazaki H, Itsweire EC (1990) Effects of turbulent shear flow on zooplankton distribution. *Deep Sea Res* 37:447–461.
11. Kimmerer WJ, Gross ES, MacWilliams ML (2014) Tidal migration and retention of estuarine zooplankton investigated using a particle-tracking model. *Limnol Oceanogr* 59:901–916.
12. Genin A, Jaffe JS, Reef R, Richter C, Franks PJS (2005) Swimming against the flow: A mechanism of zooplankton aggregation. *Science* 308:860–862.
13. Incze LS, Hebert D, Wolff N, Oakey N, Dye D (2001) Changes in copepod distributions associated with increased turbulence from wind stress. *Mar Ecol Prog Ser* 213: 229–240.
14. Schmitt FG, Devreker D, Dur G, Souissi S (2011) Direct evidence of tidally oriented behavior of the copepod *Eurytemora affinis* in the Seine estuary. *Ecol Res* 26: 773–780.
15. Kiørboe T, Jiang H, Gonçalves RJ, Nielsen LT, Wadhwa N (2014) Flow disturbances generated by feeding and swimming zooplankton. *Proc Natl Acad Sci USA* 111:11738–11743.
16. Jiang H, Kiørboe T (2011) The fluid dynamics of swimming by jumping in copepods. *J R Soc Interface* 8:1090–1103.
17. Michalec FG, Schmitt FG, Souissi S, Holzner M (2015) Characterization of intermittency in zooplankton behaviour in turbulence. *Eur Phys J E* 38:108.
18. Kiørboe T, Saiz E, Visser A (1999) Hydrodynamic signal perception in the copepod Acartia tonsa. *Mar Ecol Prog Ser* 179:97–111.
19. Buskey EJ, Strickler JR, Bradley CJ, Hartline DK, Lenz PH (2017) Escapes in copepods: Comparison between myelinate and amyelinate species. *J Exp Biol* 220:754–758.
20. Fuchs HL, Gerby GP (2016) Seascape-level variation in turbulence- and wave-generated hydrodynamic signals experienced by plankton. *Prog Oceanogr* 141: 109–129.
21. Drennan WM, Donelan MA, Terray EA, Katsaros KB (1996) Oceanic turbulence dissipation measurements in SWADE. *J Phys Oceanogr* 26:808–815.
22. Sutherland P, Melville WK (2015) Field measurements of surface and near-surface turbulence in the presence of breaking waves. *J Phys Oceanogr* 45:943–965.
23. Lozovatsky ID, Roget E, Fernando HJS, Figueroa M, Shapovalov S (2006) Sheared turbulence in a weakly stratified upper ocean. *Deep Sea Res* 53:387–407.
24. Sutherland G, Ward B, Christensen KH (2013) Wave-turbulence scaling in the ocean mixed layer. *Ocean Sci* 9:597–608.
25. Palmer MR, et al. (2015) Turbulence and mixing by internal waves in the Celtic Sea determined from ocean glider microstructure measurements. *J Mar Syst* 144:57–69.
26. Holleman RC, Geyer WR, Ralston DK (2016) Stratified turbulence and mixing efficiency in a salt wedge estuary. *J Phys Oceanogr* 46:1769–1783.
27. McMillan J, Hay A, Lueck RG, Wolk F (2016) Rates of dissipation of turbulent kinetic energy in a high Reynolds number tidal channel. *J Atmos Ocean Technol* 33:817–837.
28. Babler MU, Biferale L, Lanotte AS (2012) Breakup of small aggregates driven by turbulent hydrodynamical stress. *Phys Rev E Stat Nonlin Soft Matter Phys* 85:025301.
29. Lüthi B, Tsinober A, Kinzelbach W (2005) Lagrangian measurement of vorticity dynamics in turbulent flow. *J Fluid Mech* 528:87–118.
30. Viitasalo M, Kiørboe T, Flinkman J, Pedersen LW, Visser AW (1998) Predation vulnerability of planktonic copepods: Consequences of predator foraging strategies and prey sensory abilities. *Mar Ecol Prog Ser* 175:129–142.
31. Titelman J, Kiørboe T (2003) Predator avoidance by nauplii. *Mar Ecol Prog Ser* 247:137–149.
32. Bradley CJ, Strickler JR, Buskey EJ, Lenz PH (2013) Swimming and escape behavior in two species of calanoid copepods from Nauplius to adult. *J Plankton Res* 35:49–65.
33. Burdick DS, Hartline DK, Lenz PH (2007) Escape strategies in co-occurring calanoid copepods. *Limnol Oceanogr* 52:2373–2385.
34. Yen J, Murphy DW, Fan L, Webster DR (2015) Sensory-motor systems of copepods involved in their escape from suction feeding. *Integr Comp Biol* 55:121–133.
35. Kiørboe T, Andersen A, Langlois VJ, Jakobsen HH (2010) Unsteady motion: Escape jumps in planktonic copepods, their kinematics and energetics. *J R Soc Interface* 7:1591–1602.
36. Buskey EJ, Lenz PH, Hartline DK (2002) Escape behavior of planktonic copepods in response to hydrodynamic disturbances: High speed video analysis. *Mar Ecol Prog Ser* 235:135–146.
37. Adhikari D, Gemmell BJ, Hallberg MP, Longmire EK, Buskey EJ (2015) Simultaneous measurement of 3D zooplankton trajectories and surrounding fluid velocity field in complex flows. *J Exp Biol* 218:3534–3540.
38. Gilbert OM, Buskey EJ (2005) Turbulence decreases the hydrodynamic predator sensing ability of the calanoid copepod Acartia tonsa. *J Plankton Res* 27:1067–1071.
39. Sreenivasan KR, Bershadskii A (2006) Clustering properties in turbulent signals. *J Stat Phys* 125:1145–1157.
40. Katona SK (1973) Evidence for sex pheromones in planktonic copepods. *Limnol Oceanogr* 18:574–583.
41. Doall MH, Colin SP, Strickler JR, Yen J (1998) Locating a mate in 3D: The case of Temora longicornis. *Philos Trans R Soc B* 353:681–689.
42. Bagøien E, Kiørboe T (2005) Blind dating - mate finding in planktonic copepods. I. Tracking the pheromone trail of Centropages typicus. *Mar Ecol Prog Ser* 300: 105–115.
43. Gaylord B, Hodin J, Ferner MC (2013) Turbulent shear spurs settlement in larval sea urchins. *Proc Natl Acad Sci USA* 110:6901–6906.
44. Fuchs HL, Gerbi GP, Hunter EJ, Christman AJ, Diez FJ (2016) Hydrodynamic sensing and behavior by oyster larvae in turbulence and waves. *J Exp Biol* 218:1419–1432.
45. Wheeler JD, Helfrich KR, Anderson EJ, Mullineaux LS (2015) Isolating the hydrodynamic triggers of the dive response in eastern oyster larvae. *Limnol Oceanogr* 60:1332–1343.
46. Fuchs HL, Hunter EJ, Schmitt EL, Guazzo RA (2013) Active downward propulsion by oyster larvae in turbulence. *J Exp Biol* 216:1458–1469.
47. Colabrese S, Gustavsson K, Celani A, Biferale L (2017) Flow navigation by smart microswimmers via reinforcement learning. *Phys Rev Lett* 118:158004.
48. Gallager SM, Yamasaki H, Davis CS (2004) Contribution of fine-scale vertical structure and swimming behavior to formation of plankton layers on Georges Bank. *Mar Ecol Prog Ser* 267:27–43.
49. Lagadeuc Y, Boulé M, Dodson JJ (1997) Effect of vertical mixing on the vertical distribution of copepods in coastal waters. *J Plankton Res* 19:1183–1204.
50. Visser AW, Saitao H, Saiz E, Kiørboe T (2001) Observations of copepod feeding and vertical distribution under natural turbulent conditions in the North Sea. *Mar Biol* 138:1011–1019.
51. Visser AW, Mariani P, Pigolotti S (2009) Swimming in turbulence: Zooplankton fitness in terms of foraging efficiency and predation risk. *J Plankton Res* 31: 121–133.
52. Devreker D, et al. (2010) Tidal and annual variability of the population structure of *Eurytemora affinis* in the middle part of the Seine Estuary during 2005. *Estuar Coast Shelf Sci* 89:245–255.
53. Jiang H, Kiørboe T (2011) Propulsion efficiency and imposed flow fields of a copepod jump. *J Exp Biol* 214:476–486.
54. Gemmell BJ, Adhikari D, Longmire EK (2014) Volumetric quantification of fluid flow reveals fish's use of hydrodynamic stealth to capture evasive prey. *J R Soc Interface* 11:20130880.
55. Durham WM, Kessler JO, Stocker R (2009) Disruption of vertical motility by shear triggers formation of thin phytoplankton layers. *Science* 323:1067–1070.
56. De Lillo D, et al. (2014) Turbulent fluid acceleration generates clusters of gyrotactic microorganisms. *Phys Rev Lett* 112:044502.
57. Pigolotti S, Benzi R (2014) Selective advantage of diffusing faster. *Phys Rev Lett* 112:188102.
58. Hoyer K, et al. (2005) 3D scanning particle tracking velocimetry. *Exp Fluids* 39: 923–934.
59. Devreker D, Souissi S, Molinero JC, Nkubito F (2008) Trade-offs of the copepod *Eurytemora affinis* in mega-tidal estuaries: Insights from high frequency sampling in the Seine estuary. *J Plankton Res* 30:1329–1342.
60. Xu H, Bodenschatz E (2008) Motion of inertial particles with size larger than Kolmogorov scale in turbulent flows. *Physica D* 237:2095–2100.
61. Liberzon A, et al. (2012) On the structure of acceleration in turbulence. *Physica D* 241:208–215.
62. Maas HG, Gruen A, Papantoniou D (1993) Particle tracking velocimetry in three-dimensional flows. Part I. Photogrammetric determination of particle coordinates. *Exp Fluids* 15:133–146.
63. Malik NA, Dracos T, Papantoniou DA (1993) Particle tracking velocimetry in three-dimensional flows. Part II. Particle tracking. *Exp Fluids* 15:279–294.

64. Willneff J (2003) Some aspects of strain, vorticity and material element dynamics as measured with 3D particle tracking velocimetry in a turbulent flow. PhD thesis (ETH Zurich, Zurich).
65. Lüthi B (2002) A spatio-temporal matching algorithm for 3D particle tracking velocimetry. PhD thesis (ETH Zurich, Zurich).
66. Ott S, Mann J (2000) Velocity-acceleration structure function and Kolmogorov's 4/5 law. *Advances in Turbulence 8 Proceedings of the 12th EUROMECH European Turbulence Conference*, ed Dopazo C (CIMNE, Barcelona), pp 839–842.
67. Ishihara T, Kaneda Y, Yokokawa M, Itakura K, Uno A (2005) Energy spectrum in the near dissipation range of high resolution direct numerical simulation of turbulence. *J Phys Soc Jpn* 74:1464–1471.
68. Saha D, et al. (2016) Breakup of finite size colloidal aggregates in turbulent flow investigated by 3D particle tracking velocimetry. *Langmuir* 32:155–165.
69. Knutsen T, Melle W, Calise L (2001) Determining the mass density of marine copepods and their eggs with a critical focus on some of the previously used methods. *J Plankton Res* 23:859–873.